

The First Data Release of CNIa0.02 – A Complete Nearby (Redshift < 0.02) Sample of Type Ia
Supernova Light Curves*

PING CHEN,^{1,2} SUBO DONG,¹ C. S. KOCHANEK,^{3,4} K. Z. STANEK,^{3,4} R. S. POST,⁵
M. D. STRITZINGER,⁶ J. L. PRIETO,^{7,8} ALEXEI V. FILIPPENKO,^{9,10} JUNA A. KOLLMEIER,¹¹
BOAZ KATZ,¹² LINA TOMASELLA,¹³ AND S. BOSE^{3,4}

AND

S. BENETTI,¹³ D. BERSIER,¹⁴ THOMAS G. BRINK,⁹ DAVID A. H. BUCKLEY,¹⁵ ENRICO CAPPELLARO,¹³
N. ELIAS-ROSA,^{16,17} MORGAN FRASER,¹⁸ THOMAS W.-S. HOLOIEN,¹⁹ MARIUSZ GROMADZKI,²⁰
ERKKI KANKARE,²¹ P. LUNDQVIST,²² S. MATTILA,²³ NIDIA MORRELL,²⁴ A. PASTORELLO,¹³
B. J. SHAPPEE,²⁵ TODD A. THOMPSON,^{3,4} AND WEIKANG ZHENG⁹

¹*Kavli Institute for Astronomy and Astrophysics, Peking University, Yi He Yuan Road 5, Hai Dian District, Beijing 100871, China*

²*Department of Astronomy, School of Physics, Peking University, Yi He Yuan Road 5, Hai Dian District, Beijing 100871, China*

³*Department of Astronomy, The Ohio State University, 140 West 18th Avenue, Columbus, OH 43210, USA*

⁴*Center for Cosmology and Astroparticle Physics, The Ohio State University, 191 W. Woodruff Avenue, Columbus, OH 43210, USA*

⁵*Post Observatory, Lexington, MA 02421, USA*

⁶*Department of Physics and Astronomy, Aarhus University, Ny Munkegade 120, DK-8000 Aarhus C, Denmark*

⁷*Núcleo de Astronomía de la Facultad de Ingeniería y Ciencias, Universidad Diego Portales, Av. Ejército 441, Santiago, Chile*

⁸*Millennium Institute of Astrophysics, Santiago, Chile*

⁹*Department of Astronomy, University of California, Berkeley, CA 94720-3411, USA*

¹⁰*Miller Senior Fellow, Miller Institute for Basic Research in Science, University of California, Berkeley, CA 94720, USA*

¹¹*Observatories of the Carnegie Institution for Science, 813 Santa Barbara Street, Pasadena, CA 91101, USA*

¹²*Department of Particle Physics and Astrophysics, Weizmann Institute of Science, Rehovot 76100, Israel*

¹³*INAF - Osservatorio Astronomico di Padova, Vicolo dell'Osservatorio 5, I-35122 Padova, Italy*

¹⁴*Astrophysics Research Institute, Liverpool John Moores University, 146 Brownlow Hill, Liverpool L3 5RF, UK*

¹⁵*South African Astronomical Observatory, P.O. Box 9, Observatory 7935, Cape Town, South Africa*

¹⁶*Institute of Space Sciences (ICE, CSIC), Campus UAB, Carrer de Can Magrans s/n, 08193 Barcelona, Spain*

¹⁷*Institut d'Estudis Espacials de Catalunya (IEEC), c/Gran Capitá 2-4, Edif. Nexus 201, 08034 Barcelona, Spain*

¹⁸*School of Physics, O'Brien Centre for Science North, University College Dublin, Belfield, Dublin 4, Ireland*

¹⁹*The Observatories of the Carnegie Institution for Science, 813 Santa Barbara St., Pasadena, CA 91101, USA*

²⁰*Astronomical Observatory, University of Warsaw, Al. Ujazdowskie 4, 00-478 Warszawa, Poland*

²¹*Department of Physics and Astronomy, University of Turku, FI-20014 Turku, Finland*

²²*The Oskar Klein Centre, Department of Astronomy, Stockholm University, AlbaNova, SE-10691, Stockholm, Sweden*

²³*Tuorla observatory, Department of Physics and Astronomy, University of Turku, FI-20014 Turku, Finland*

²⁴*Las Campanas Observatory, Carnegie Observatories, Casilla 601, La Serena, Chile*

Corresponding author: Subo Dong
dongsubo@pku.edu.cn

* This paper includes data gathered with the 6.5 meter Magellan Telescopes located at Las Campanas Observatory, Chile.

²⁵*Institute for Astronomy, University of Hawaii, 2680 Woodlawn Drive, Honolulu, HI 96822, USA*

ABSTRACT

The CN1a0.02 is a complete, nearby sample of Type Ia supernova (SN Ia) multiband light curves, and it is volume-limited with host-galaxy redshift $z_{\text{host}} < 0.02$. The scientific goal of CN1a0.02 is to infer the distributions of key properties (e.g., the luminosity function) of local SNe Ia in a complete and unbiased fashion in order to study SN explosion physics. We spectroscopically classify any SN candidate detected (discovered or recovered) by the All-Sky Automated Survey for Supernovae (ASAS-SN) that reaches peak brightness < 16.5 mag. Since ASAS-SN scans the full sky and does not target specific galaxies, the sample is effectively unbiased by host-galaxy properties. We obtain multiband photometric observations starting from the time of discovery. In the first data release (DR1), we present the optical light curves obtained for 240 SNe (including 182 with multiband data), and we derive parameters such as the peak fluxes and Δm_{15} .

Keywords: supernovae: general

1. INTRODUCTION

The explosion mechanism and progenitors of Type Ia supernovae (SNe Ia) are basic but open questions in astrophysics. There are several proposed channels, but no agreement as to which or even how many of the channels dominate (see, e.g., Maoz et al. 2014). SNe Ia span about an order of magnitude in peak luminosities and in the masses of synthesized ^{56}Ni that power the radiation. It is also debated whether this range in properties represents one continuous population or several overlapping but distinct populations. On the one hand, the main properties of SNe Ia appear to be continuous across the whole luminosity range. Phillips (1993) found that the peak luminosity of SNe Ia is tightly correlated with the light-curve shape characterized by the B -band post-peak decline rate $\Delta m_{15}(B)$, and this width-luminosity relation (WLR) is the foundation for using SNe Ia as cosmological distance indicators. Many properties of their light curves (see, e.g., Phillips 2012; Burns et al. 2014; Bulla et al. 2020) and spectra (see, e.g., Nugent et al. 1995; Branch et al. 2009) also seem to be continuous. On the other hand, there is some evidence for bimodality in the luminosity function (via the proxy of $\Delta m_{15}(B)$) (e.g., Ashall et al. 2016) and distinct ultraviolet (UV)-optical (Milne et al. 2013) and early-time optical colors (Stritzinger et al. 2018).

There have been tremendous efforts to obtain high-quality multiband light curves of large samples of nearby SNe Ia (e.g., Hamuy et al. 1996; Riess et al. 1999; Jha et al. 2006; Hicken et al. 2009; Ganeshalingam et al. 2010; Contreras et al. 2010; Stritzinger et al. 2011; Hicken et al. 2012; Krisciunas et al. 2017; Foley et al. 2018; Stahl et al. 2019). However, collecting a complete and unbiased nearby sample has only been made possible recently, thanks to the advent of wide-field time-domain surveys that do not target specific galaxies, such as the All-Sky Automated Survey for SuperNovae (ASAS-SN; Shappee et al. 2014; Kochanek et al. 2017), the *Gaia* transient survey (Hodgkin et al. 2013), the Palomar Transient Factory (Law et al. 2009) and its successor the Zwicky Transient Facility (ZTF; Kulkarni 2016; Perley et al. 2020) and its predecessors, the Asteroid Terrestrial-impact Last Alert System (ATLAS; Tonry 2011; Tonry et al. 2018), the Mobile Astronomical System of Telescope Robots (MASTER; Gorbovskey et al. 2013), OGLE Transients Detection System (OTDS;

Wyrzykowski et al. 2014), the Pan-STARRS Survey for Transients (PSST; Huber et al. 2015), and the Catalina Real-Time Transient Survey (CRTS; Drake et al. 2009).

We carry out the CN1a0.02 program to collect a **C**omplete, **N**earby, and effectively unbiased sample of Type **Ia** Supernovae at host-galaxy redshifts $z_{\text{host}} < 0.02$ with well-observed multiband light curves. Our follow-up observations started in January 2015 and ended in January 2020, and the SNe observed between 2015 June 13 and 2019 January 31 were selected following the criteria of the complete sample. The goal for constructing a complete sample that is unbiased toward host-galaxy properties is to enable reliable statistical inference on the distributions of photometric properties of SNe Ia (e.g., luminosity, color, light-curve shape, and derived physical parameters) in the local universe and to study the dependence of these on host-galaxy properties.

The complete sample includes all SNe Ia that meet our selection criteria of host-galaxy redshifts $z < 0.02$, peak brightness $V < 16.5$ mag and discovered or recovered by the ASAS-SN survey. By recovered, we mean an SN discovered first by another survey or an individual that would otherwise have been discovered by ASAS-SN. Holoien et al. (2017a,b,c, 2019) have shown that with these limits the ASAS-SN sample has very high completeness and minimal bias in host-galaxy properties or SN locations inside the hosts. All of the SNe have been spectroscopically classified by ASAS-SN or other groups. Where host-galaxy redshifts were unavailable, we have also measured those directly. All of the SNe were followed photometrically, mainly in the $BVri$ bands, but with near-infrared (IR) and *Swift* UV observations of some objects as well. In this first data release (DR1) of CN1a0.02, we present optical light curves for 240 SNe Ia observed between 2015 and 2020. We describe the overall program in Section 2, the data processing in Section 3, and the resulting light curves in Section 4. Our present results are summarized in Section 5.

2. PROGRAM DESCRIPTION

We select our sources primarily based on ASAS-SN detections, which not only include ASAS-SN discoveries, but also discoveries by others that were later recovered by ASAS-SN. The complete sample was collected between 2015 June 13 and 2019 January 31. We have also observed a few SNe Ia before (since January 2015) and after this period (until January 2020), but they are not part of the complete sample. In the first phase of the complete sample collection, we attempted to observe all SNe Ia with $z < 0.034$ and a peak magnitude of $V < 17$. Between October 2016 and January 2019, we restricted the sample to focus on SNe Ia with $z < 0.02$ and a peak magnitude of $V < 16.5$ as shown in Fig. 4 and discussed in Appendix A. The detection efficiency of the ASAS-SN survey has been evolving mainly owing to upgrades in hardware, and since 2015, the detection efficiency has been nearly 100% complete to < 16.5 mag. The complete sample consists only of those with $z < 0.02$ and peak $V < 16.5$ mag. Note that SNe Ia on the WLR span a luminosity range of $-19.5 \lesssim M_V \lesssim -17$ (see, e.g., Burns et al. 2018), and due to the peak magnitude limits, our sample is not sensitive to all dim SNe Ia with $M_V \gtrsim -18.2$ within the volume confined by $z < 0.02$.

CN1a0.02 DR1 includes V -band and g -band photometry from the 14 cm telescopes used in ASAS-SN survey. We have performed photometric follow-up observations using a number of telescopes ranging from 0.3 m to ~ 2 m. In this data release, most optical data are in $BVri$ observed by 1 m telescopes in the Las Cumbres Observatory Global Telescope network (LCOGT; Brown et al. 2013) distributed in four sites covering both hemispheres, two 0.6 m telescopes in SRO (CA, USA) and Mayhill (NM, USA) of the Post Observatory, and the 1.3 m Small & Moderate Aperture Research Telescope System (SMARTS; Subasavage et al. 2010). We also include some photometry using OSMOS on the 2.4 m

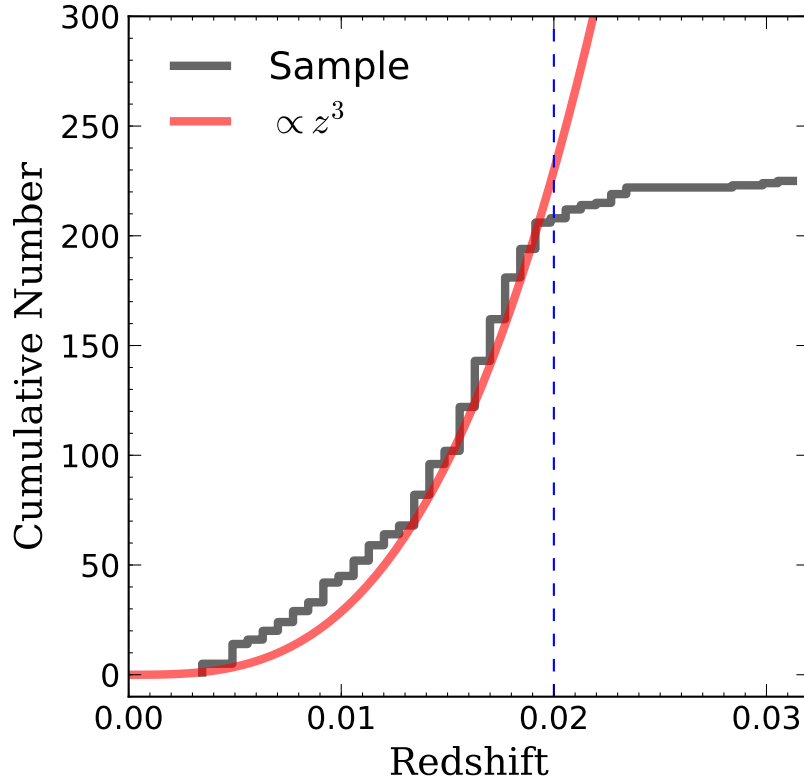


Figure 1. Cumulative redshift distribution of the SNe Ia in CNIa0.02 (black); the completeness cut is indicated with a blue dashed vertical line. An illustrative red line of $N \propto z^3$ is plotted to indicate the expectation from a volume-limited sample and assuming a linear relation between distance and redshift.

Hiltner Telescope at the MDM observatory, WFCCD on the 2.5 m Du Pont telescope, and ALFOSC on the 2.56 m Nordic Optical Telescope (NOT). Data from other facilities will be made available in future data releases.

We start multiband photometric observations immediately after the discovery of the SN candidate, regardless of whether a spectroscopic classification is available. For most objects, this data release contains follow-up photometry ending around 40–60 days after the optical peak. For objects with a bright galaxy background that require image subtractions, we take template images at least 300 days after B -band peak, when the SN is generally $\gtrsim 7$ mag below the peak. There are 34 SNe observed by the above-mentioned facilities that do not have satisfactory template images; we will take templates and publish their follow-up light curves in a future data release.

3. DATA PROCESSING

This data release contains the results of processing over 20,000 images. We developed a Python photometric pipeline *PmPyeasy*¹ to automatically process the images and obtain the photometry. The pipeline utilizes several external software packages that are all wrapped in a clean Python

¹ <https://github.com/AtomyChan/PmPyeasy>

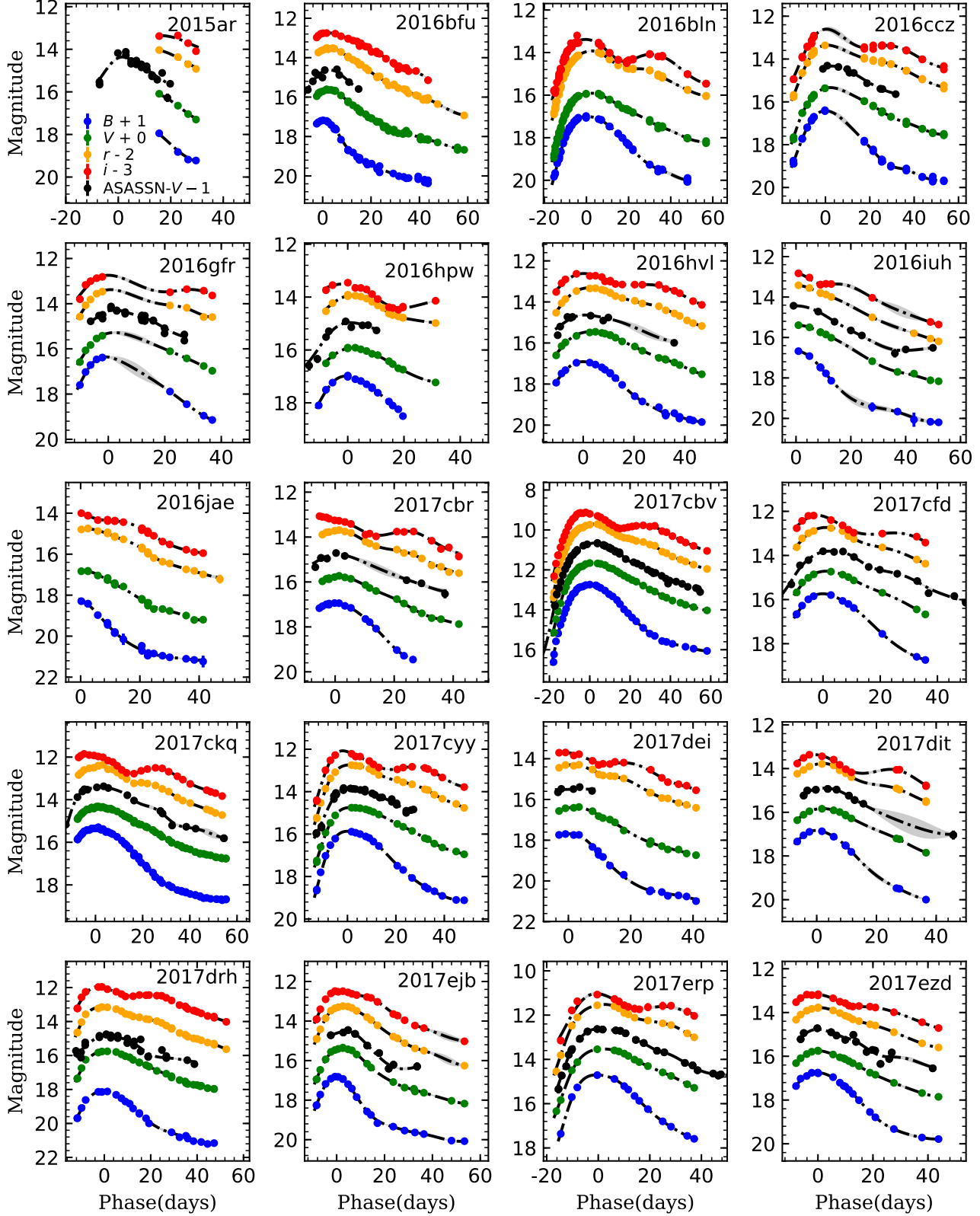


Figure 2. Multiband light curves of SNe Ia in CNIa0.02 DR1. The black dash-dotted lines correspond to Gaussian Process fits (see Section 4.2 for details). All dates are relative to the time of B -band maximum brightness where determined or otherwise to the discovery time.

(A full version of this figure with all SNe Ia presented in this work will be available in the online journal.)

interface. The pipeline runs automatically by default, but allows manual operations at any point when necessary. The pipeline uses *pyds9*² to facilitate human inspections through XPA messaging to SAOImageDS9³. It takes images that have already been pre-processed including bias removal and flat fielding. Here we outline the processing steps.

3.1. Image Registration and Source Detection

The pipeline distributes all the images to object-specific folders and adds information such as the filter, exposure time, and epoch to a database. Next, it removes cosmic rays using an implementation of L.A. Cosmic technique (van Dokkum 2001), measures the full width at half-maximum intensity (FWHM) of the stellar profiles, and estimates the background value for each image. It then employs *PyRAF daofind* to generate a source catalog for each image.

3.2. PSF Photometry and Image Subtraction

We perform point-spread-function (PSF) photometry for SNe that have negligible host-galaxy contamination using DoPHOT (Schechter et al. 1993; Alonso-García et al. 2012). DoPHOT generates a PSF model automatically and obtains magnitudes for all sources that meet the given criteria.

A large number of targets have significant galaxy background flux and require image subtraction. To perform image subtraction, the pipeline first matches point sources detected in the science image and the template image, and then the science image is astrometrically aligned to the template image using the matched sources and resampled. The image subtraction is done with the High Order Transform of PSF ANd Template Subtraction package (HOTPANTS; Becker 2015). The FWHMs of the template and resampled science image are used to determine the convolution direction: images with better seeing are convolved with the kernel for subtraction. We configured HOTPANTS to normalize the fluxes measured on all subtracted images to the flux scale of the template system.

To perform photometry, the pipeline first identifies isolated stars with high signal-to-noise ratios (SNRs) in the template image, and these stars are used to build a PSF model for each convolved image. Then PSF photometry is performed on the subtracted image at the SN position and for all the sources in the template image using the *PyRAF daophot* task.

3.3. Photometric Calibration

For the photometric calibration, the first step is to calibrate the instrumental magnitudes in the appropriate natural system of a certain telescope/CCD/filter set. The photometric standards are selected from the Pan-STARRS1 DR1 MeanObject database table (Flewelling et al. 2016) or the ATLAS All-Sky Stellar Reference Catalog (Refcat2, Tonry et al. 2018) and transformed to the standard Johnson *BV* and SDSS *ri* bands as detailed in Appendix C. Then they are converted to the appropriate natural systems:

$$B_{\text{nat}} = B_{\text{std}} + CT_B \times (B_{\text{std}} - V_{\text{std}}), \quad (1)$$

$$V_{\text{nat}} = V_{\text{std}} + CT_V \times (B_{\text{std}} - V_{\text{std}}), \quad (2)$$

$$r_{\text{nat}} = r_{\text{std}} + CT_r \times (r_{\text{std}} - i_{\text{std}}), \text{ and} \quad (3)$$

$$i_{\text{nat}} = i_{\text{std}} + CT_i \times (r_{\text{std}} - i_{\text{std}}), \quad (4)$$

² <http://hea-www.harvard.edu/RD/pyds9/>

³ <https://sites.google.com/cfa.harvard.edu/saoimageds9>

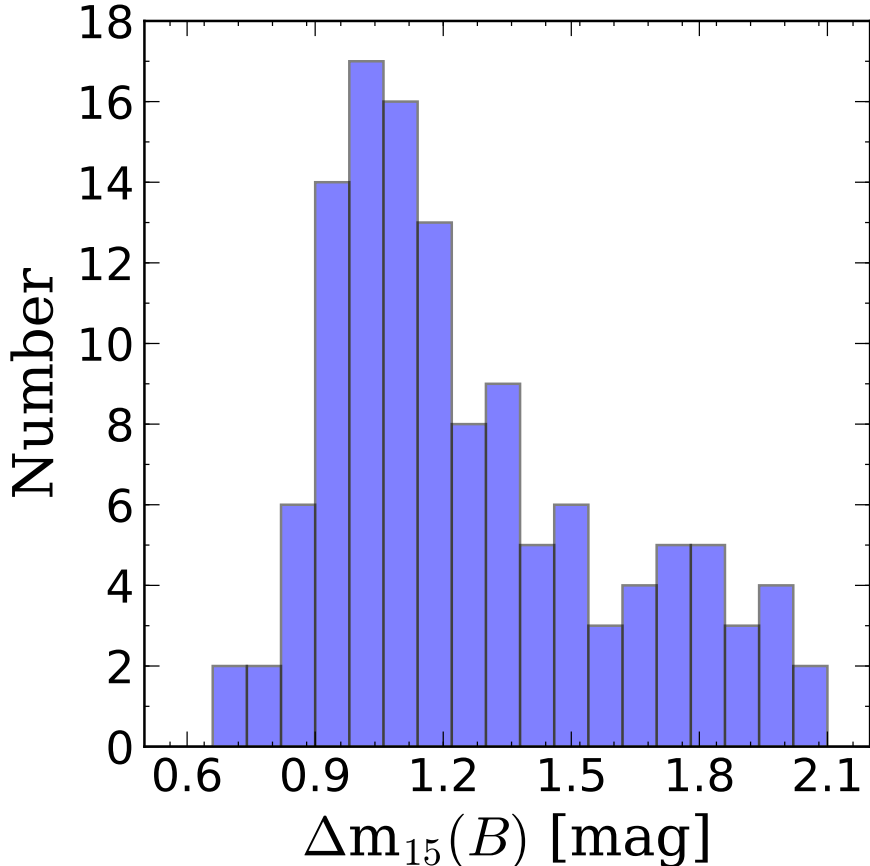


Figure 3. $\Delta m_{15}(B)$ distribution of SNe Ia in CNIa0.02 DR1.

where CT_X are the color terms (X stands for B , V , r , and i). The offsets between instrumental magnitudes and magnitudes in the natural system ($m_{\text{offset}} = m_{\text{nat}} - m_{\text{inst}}$) are computed, and the instrumental magnitudes are then transformed to the corresponding natural system.

In practice, for PSF photometry, the source instrumental magnitudes are matched to those in the catalog of standards to derive zeropoints (ZP_X) and color terms (CT_X) for the corresponding telescope/CCD/filter set. This solution is derived by fitting $m_{\text{diff}} = CT_X \times \text{Color} + ZP_X$. For image-subtraction photometry, all instrumental magnitudes are in the same photometric system as the template, so the determination of photometric zero points is only performed on the template image.

The second step of photometric calibration is to transform magnitudes in the natural system to the corresponding standard system. For each telescope/CCD/filter set, this is done by inverting the Equations 1–4 and using the appropriate color terms. In this iterative process for each image, the observed color of the SN is required in standard system at the epoch of observation. The typical uncertainty of our calibrated photometry is ~ 0.05 mag.

4. RESULTS

In Table 1, we give the general information (survey names, IAU names, equatorial coordinates, host-galaxy names, and heliocentric host redshifts) for objects that have follow-up data (regardless of whether they belong to the complete sample) or have been considered for follow-up observations (regardless of whether such data are obtained). We also provide additional information (discovery

date, brightest observed magnitude, and whether detected by ASAS-SN) which can be used to check whether an object meets the selection criteria of complete sample (i.e., in the date range of 2015 June 13 and 2019 January 31, peak brightness < 16.5 mag and detected by ASAS-SN) in addition to the redshift cut ($z_{\text{host}} < 0.02$). The host-galaxy redshifts are from either the NASA/IPAC Extragalactic Database (NED) or new measurements presented in Table 2. There are 11 SNe whose host-galaxy redshifts are not yet available (indicated with asterisk marks), and we plan to measure them in the future. A cumulative distribution of host-galaxy redshifts for the objects is shown in Figure 1, which roughly follows the expectation for a volume-limited complete sample when peculiar velocity is negligible compared to the Hubble expansion velocity (at $z \gtrsim 0.01$). Since we are not sensitive to all SNe Ia at the dim end of the luminosity function ($\gtrsim -18.2$) at $z = 0.02$, so our sample is not expected to exactly follow the distribution of a volume-limited complete sample.

4.1. Light-Curve Data

In this section, we present the optical light curves of 240 SNe Ia. These data include Vg -band light curves from ASAS-SN observations using image subtraction (see more descriptions in Jayasinghe et al. 2018). We have successfully conducted $BVri$ follow-up observations of 216 SNe, and we present light curves for all of them except for 34 objects that require image-subtraction photometry but do not have satisfactory templates available yet. $BVri$ light curves from follow-up observations were conducted by LCOGT, Post Observatory, and SMARTS, as well as a small number of relatively late-phase data from Hiltner, Du Pont, and NOT. The light curves of SNe Ia up to 60 days past B -band peak or discovery time (if peak time is not available) are displayed in Figure 2. The corresponding photometry results in the natural systems are provided in Table 3.

4.2. Basic Light-Curve Parameters

We perform simple fits to the well-covered SN Ia light curves to derive basic parameters such as the time and magnitude of peak brightness and the decline rates in the B and V bands. The decline rate $\Delta m_{15}(X)$ (Phillips 1993) refers to the magnitude decline within 15 days after peak brightness in a given filter. We measure these parameters directly from the interpolated light curves in each band X (BV) using a Gaussian process regression method. Gaussian process regression is a powerful tool in handling time-series data, having the advantage of allowing for the inclusion of uncertainty information and producing relatively unbiased estimates of interpolated values (see, e.g., Lochner et al. 2016). The results are given in Table 4. Note that the fitting is done without making host-galaxy extinction corrections, which may affect the derived Δm_{15} for objects with high extinction (Phillips et al. 1999).

Figure 3 shows the histogram of the $\Delta m_{15}(B)$ distribution of the objects in this data release. As can be seen, we have objects spanning the whole range of $\Delta m_{15}(B)$ of the SN Ia population from $\Delta m_{15}(B) \approx 0.7$ mag to $\Delta m_{15}(B) \approx 2.0$ mag. Further work on quantifying detection efficiency needs to be carried out to obtain the intrinsic distribution of $\Delta m_{15}(B)$ for CNIa0.02.

5. SUMMARY

The goal of CNIa0.02 is to produce a complete and unbiased sample of nearby SNe Ia with multiband light curves that sample the whole population of SNe Ia. We present 240 SNe with optical light curves in this data release. We expect to also publish near-UV, near-IR, and late-phase photometric data in the future data releases. When completed, the sample will provide a large and homogeneous dataset

to infer the intrinsic distribution properties of SNe Ia in the local universe, which will ultimately help answer basic questions regarding SN Ia progenitor systems and explosion mechanisms.

We acknowledge the Telescope Access Program (TAP) funded by the NAOC, CAS and the Special Fund for Astronomy from the Ministry of Finance. CSK, KZS and BJS are supported by NSF grants AST-1515927, AST-1814440, and AST-1908570. M.D.S acknowledges funding from the Vilum Fonden (project numbers 13261 and 28021). A.V.F.’s supernova group is grateful for financial assistance from the Christopher R. Redlich Fund, the TABASGO Foundation, and the Miller Institute for Basic Research in Science (U.C. Berkeley). A major upgrade of the Kast spectrograph on the Shane 3 m telescope at Lick Observatory was made possible through generous gifts from William and Marina Kast as well as the Heising-Simons Foundation. Research at Lick Observatory is partially supported by a generous gift from Google. We thank the staffs of the various observatories at which data were obtained for their excellent assistance. JLP is provided in part by FONDECYT through the grant 1191038 and by the Ministry of Economy, Development, and Tourism’s Millennium Science Initiative through grant IC120009, awarded to The Millennium Institute of Astrophysics, MAS. MF acknowledges the support of a Royal Society - Science Foundation Ireland University Research Fellowship. BJS is also supported by NSF grants AST-1920392 and AST-1911074. MG is supported by the Polish NCN MAESTRO grant 2014/14/A/ST9/00121. Polish participation in SALT is funded by grant no. MNiSW DIR/WK/2016/07.

Software: Astropy (Astropy Collaboration et al. 2018), PyRAF (Science Software Branch at STScI 2012), FITSH (Pál 2012), ccdproc (Craig et al. 2017)

REFERENCES

- Alonso-García, J., Mateo, M., Sen, B., et al. 2012, *AJ*, 143, 70
- Ashall, C., Mazzali, P., Sasdelli, M., & Prentice, S. J. 2016, *MNRAS*, 460, 3529
- Astropy Collaboration, Price-Whelan, A. M., Sipócz, B. M., et al. 2018, *AJ*, 156, 123
- Becker, A. 2015, HOTPANTS: High Order Transform of PSF AND Template Subtraction, ascl:1504.004
- Branch, D., Chau Dang, L., & Baron, E. 2009, *PASP*, 121, 238
- Brown, T. M., Baliber, N., Bianco, F. B., et al. 2013, *PASP*, 125, 1031
- Bulla, M., Miller, A. A., Yao, Y., et al. 2020, *ApJ*, 902, 48
- Burns, C. R., Stritzinger, M., Phillips, M. M., et al. 2014, *ApJ*, 789, 32
- Burns, C. R., Parent, E., Phillips, M. M., et al. 2018, *ApJ*, 869, 56
- Chambers, K. C., Magnier, E. A., Metcalfe, N., et al. 2016, arXiv e-prints, arXiv:1612.05560
- Contreras, C., Hamuy, M., Phillips, M. M., et al. 2010, *AJ*, 139, 519
- Craig, M., Crawford, S., Seifert, M., et al. 2017, astropy/ccdproc: v1.3.0.post1, doi:10.5281/zenodo.1069648
- DePoy, D. L., Atwood, B., Belville, S. R., et al. 2003, in Proc. SPIE, Vol. 4841, Instrument Design and Performance for Optical/Infrared Ground-based Telescopes, ed. M. Iye & A. F. M. Moorwood, 827–838
- Drake, A. J., Djorgovski, S. G., Mahabal, A., et al. 2009, *ApJ*, 696, 870
- Flewelling, H. A., Magnier, E. A., Chambers, K. C., et al. 2016, arXiv e-prints, arXiv:1612.05243
- Foley, R. J., Scolnic, D., Rest, A., et al. 2018, *MNRAS*, 475, 193
- Fukugita, M., Ichikawa, T., Gunn, J. E., et al. 1996, *AJ*, 111, 1748
- Ganeshalingam, M., Li, W., Filippenko, A. V., et al. 2010, *ApJS*, 190, 418

- Gorbovskoy, E. S., Lipunov, V. M., Kornilov, V. G., et al. 2013, *Astronomy Reports*, 57, 233
- Hamuy, M., Phillips, M. M., Suntzeff, N. B., et al. 1996, *AJ*, 112, 2391
- Hicken, M., Challis, P., Jha, S., et al. 2009, *ApJ*, 700, 331
- Hicken, M., Challis, P., Kirshner, R. P., et al. 2012, *ApJS*, 200, 12
- Hodgkin, S. T., Wyrzykowski, L., Blagorodnova, N., & Koposov, S. 2013, *Philosophical Transactions of the Royal Society of London Series A*, 371, 20120239
- Holoien, T. W. S., Stanek, K. Z., Kochanek, C. S., et al. 2017a, *MNRAS*, 464, 2672
- Holoien, T. W. S., Brown, J. S., Stanek, K. Z., et al. 2017b, *MNRAS*, 467, 1098
- . 2017c, *MNRAS*, 471, 4966
- Holoien, T. W. S., Brown, J. S., Vallely, P. J., et al. 2019, *MNRAS*, 484, 1899
- Huber, M., Carter Chambers, K., Flewelling, H., et al. 2015, in *IAU General Assembly*, Vol. 29, 2258303
- Jayasinghe, T., Kochanek, C. S., Stanek, K. Z., et al. 2018, *MNRAS*, 477, 3145
- Jha, S., Kirshner, R. P., Challis, P., et al. 2006, *AJ*, 131, 527
- Kochanek, C. S., Shappee, B. J., Stanek, K. Z., et al. 2017, *PASP*, 129, 104502
- Krisciunas, K., Contreras, C., Burns, C. R., et al. 2017, *AJ*, 154, 211
- Kulkarni, S. R. 2016, in *American Astronomical Society Meeting Abstracts*, Vol. 227, *American Astronomical Society Meeting Abstracts #227*, 314.01
- Landolt, A. U. 1992, *AJ*, 104, 340
- Law, N. M., Kulkarni, S. R., Dekany, R. G., et al. 2009, *PASP*, 121, 1395
- Lochner, M., McEwen, J. D., Peiris, H. V., Lahav, O., & Winter, M. K. 2016, *ApJS*, 225, 31
- Maoz, D., Mannucci, F., & Nelemans, G. 2014, *ARA&A*, 52, 107
- Milne, P. A., Brown, P. J., Roming, P. W. A., Bufano, F., & Gehrels, N. 2013, *ApJ*, 779, 23
- Nugent, P., Phillips, M., Baron, E., Branch, D., & Hauschildt, P. 1995, *ApJL*, 455, L147
- Pál, A. 2012, *MNRAS*, 421, 1825
- Perley, D. A., Fremling, C., Sollerman, J., et al. 2020, arXiv e-prints, arXiv:2009.01242
- Phillips, M. M. 1993, *ApJL*, 413, L105
- . 2012, *PASA*, 29, 434
- Phillips, M. M., Lira, P., Suntzeff, N. B., et al. 1999, *AJ*, 118, 1766
- Riess, A. G., Kirshner, R. P., Schmidt, B. P., et al. 1999, *AJ*, 117, 707
- Schechter, P. L., Mateo, M., & Saha, A. 1993, *PASP*, 105, 1342
- Science Software Branch at STScI. 2012, *PyRAF: Python alternative for IRAF*, ascl:1207.011
- Shappee, B. J., Prieto, J. L., Grupe, D., et al. 2014, *ApJ*, 788, 48
- Stahl, B. E., Zheng, W., de Jaeger, T., et al. 2019, *MNRAS*, 490, 3882
- Stritzinger, M. D., Phillips, M. M., Boldt, L. N., et al. 2011, *AJ*, 142, 156
- Stritzinger, M. D., Shappee, B. J., Piro, A. L., et al. 2018, *ApJL*, 864, L35
- Subasavage, J. P., Bailyn, C. D., Smith, R. C., et al. 2010, in *Proc. SPIE*, Vol. 7737, *Observatory Operations: Strategies, Processes, and Systems III*, 77371C
- Tonry, J. L. 2011, *PASP*, 123, 58
- Tonry, J. L., Stubbs, C. W., Lykke, K. R., et al. 2012, *ApJ*, 750, 99
- Tonry, J. L., Denneau, L., Flewelling, H., et al. 2018, *ApJ*, 867, 105
- van Dokkum, P. G. 2001, *PASP*, 113, 1420
- Wyrzykowski, L., Kostrzewa-Rutkowska, Z., Kozłowski, S., et al. 2014, *AcA*, 64, 197

Table 1. General Properties of SNe Ia in the Sample

Survey Name	IAU Name	RA(J2000)	Dec(J2000)	Discovery Date	Host Galaxy	z_{host}^a	V_{max}^b	ASAS-SN? ^c
ASASSN-15aj		10:52:53.261	-32:55:34.86	2015-01-08	NGC 3449	0.010921	16.66	Y
ASASSN-15ak		00:12:01.546	+26:23:37.284	2015-01-09	UGC 00110	0.015034	14.69	Y
ASASSN-15db		15:46:58.69	+17:53:02.22	2015-02-15	NGC 5996	0.010998	16.6	Y
ASASSN-15eb		08:06:07.399	-22:33:48.852	2015-02-26	ESO 561- G 012	0.016481	15.68	Y
PSN J07361576-6930230	2015F	07:36:15.76	-69:30:23.0	2015-03-09	NGC2442	0.00489	13.34	Y
PSN J15053007+0138024	2015bp	15:05:30.09	+01:38:02.2	2015-03-16	NGC 5839	0.004069	13.88	Y
ASASSN-15ga		12:59:27.293	+14:10:15.78	2015-03-30	NGC 4866	0.006631	17.27	Y
ASASSN-15go		06:11:30.401	-16:29:04.596	2015-04-06	WISEA J061130.50-162908.3	0.018923	15.76	Y
ASASSN-15gw		14:16:23.971	+39:30:09.036	2015-04-10	NGC 5536	0.019507	16.42	Y
ASASSN-15he		16:31:33.66	-67:52:01.992	2015-04-12	ESO 069- G 005	0.015881	15.51	Y
ASASSN-15hf		10:29:30.835	-35:15:34.812	2015-04-17	ESO 375- G 04	0.006178	14.27	Y
ASASSN-15hx		13:43:16.69	-31:33:21.5	2015-04-26	uncatalog	0.0081	13.37	Y
ASASSN-15ih		09:59:59.570	-02:53:16.368	2015-05-06	WISEA J095959.65-025324.8	0.019827	15.83	Y
ASASSN-15jo		14:06:44.73	-34:27:18.0	2015-05-20	6dF J1406512-342931	0.015584	15.36	Y
ASASSN-15kg		08:40:12.11	-04:35:29.0	2015-05-27	6dF J0840116-043537	0.014257	15.16	Y
ASASSN-15kk		09:18:31.061	+74:19:07.536	2015-06-05	UGC 04883	0.009893	14.06	Y
ASASSN-15kp		12:58:41.7	-32:07:28.7	2015-06-07	AM 1255-315	0.017402	15.52	Y
ASASSN-15kx		22:16:11.810	+37:28:26.112	2015-06-10	MCG +06-49-001	0.018019	16.09	Y
ASASSN-15lp		01:49:10.32	+05:38:23.316	2015-06-20	MRK 0576	0.017686	15.06	Y
PSN J11492548-0507138		11:49:25.48	-05:07:13.8	2015-06-29	NGC 3915	0.005573	13.24	Y
ASASSN-15mc		02:48:59.570	+03:10:10.488	2015-07-05	UGC 02295	0.013916	15.06	Y
ASASSN-15ml		20:03:01.670	-21:54:48.24	2015-07-12	2MASX J20030163-2154516	0.018623	16.56	Y
PSN J02062253-5201267	2015aw	02:06:22.53	-52:01:26.69	2015-07-12	ESO 197- G 024	0.01962	15.55	Y
ASASSN-15od		02:23:13.210	-04:31:02.064	2015-08-10	MCG -01-07-004	0.017989	15.31	Y
ASASSN-15oh		22:30:41.976	+39:17:35.232	2015-08-14	MCG +06-49-027	0.016835	16.15	Y
ASASSN-15ol		01:54:06.041	-56:41:42.504	2015-08-15	NGC 0745 NED01	0.019777	15.57	Y
ASASSN-15pl		02:30:23.24	-20:41:00.0	2015-09-11	ESO 545- G 025	0.016165	15.12	Y
ASASSN-15pz		03:08:48.45	-35:13:51.0	2015-09-27	ESO 357- G 005	0.014903	14.23	Y
ASASSN-15qc		00:39:17.94	+03:57:00.612	2015-10-01	UGC 00402	0.017649	15.6	Y
PSN J01505356-3600308	2015ao	1:50:53.56	-36:00:30.8	2015-10-06	ESO 354- G 003	0.019133	16.81	N
MASTER OT J103747.94-270507.2	2015dc	10:37:47.94	-27:05:07.2	2015-10-20	IC 2597	0.007562	17.21	N
ASASSN-15rq		00:08:03.09	-36:33:51.7	2015-10-21	MRSS 349-038278	0.02307	15.43	Y
ASASSN-15rw		2:15:58.45	+12:14:13.812	2015-10-24	WISEA J021558.50+121414.4	0.01884	15.50	Y

^a Host-galaxy heliocentric redshifts taken from the NASA/IPAC Extragalactic Database (NED) or from new measurements in Table ???. If Host-galaxy redshift is not available, then SN redshift is displayed here instead and indicated with asterisk.

^b Brightest observed magnitude in V band.

^c Whether the SN was detected by ASAS-SN survey.

Notes. A portion is shown here for guidance regarding its form and content, and the full table will be available in its entirety in machine-readable format after acceptance to journal.

Table 2. Updated Redshifts for SNe Ia without Archival Host Redshift

SN	z_{SN}	z_{host}	Instrument
2016asf	0.021	0.018019	F18 ^a
2016blc	0.012	0.01285	F18 ^a
2016cyl	0.016	0.01646	Magellan/LDSS3
2016daj	0.032	0.03026	P200/DBSP
2016dxv	0.02	0.02431	P200/DBSP
2016gfr	0.014	0.01671	P200/DBSP
2016gou	0.016	0.0155	P200/DBSP
2016gsn	0.018	0.01505	P200/DBSP
2016gtr	0.014	0.02033	Magellan/IMACS
2016hpw	0.02	0.02102	P200/DBSP
2016hsc	0.007	0.0145	Magellan/IMACS
2016iil	0.024	0.0289	Magellan/IMACS
2017azw	0.02	0.01616	Magellan/LDSS3
2017gup	0.016	0.02316	P200/DBSP
2017h jy	0.007	0.0177	MDM/OSMOS
2017hoq	0.02	0.02341	MDM/OSMOS
2017iyw	0.0215	0.0174	MDM/OSMOS
2018aye	0.017	0.0223	P200/DBSP
2018cuh	0.012	0.01411	Magellan/LDSS3
2018enc	0.017	0.02389	Magellan/LDSS3
2018fnq	0.019	0.01906	Magellan/LDSS3
2018fop	0.02	0.02121	Magellan/LDSS3
2018ilu	0.007	0.01807	GTC/OSIRIS
2018jmo	0.02	0.0209	Shane/KAST
2018vw	0.02	0.0220	VLT/FORS2
ASASSN-15hx	n/a	0.00812	Magellan/IMACS
ASASSN-15rq	0.025	0.02307	Magellan/LDSS3
ASASSN-15rw	0.02	0.01884	F18 ^a
ASASSN-15ti	0.016	0.01732	F18 ^a
ASASSN-15uh	0.0135	0.01489	LBT/MODS

^aHost redshifts are obtained from the Foundation Supernova Survey (Foley et al. 2018)

Table 3. Optical Photometry Results

JD	<i>B</i>	<i>V</i>	<i>R</i>	<i>g</i>	<i>r</i>	<i>i</i>	Source
−2,457,000	(mag)	(mag)	(mag)	(mag)	(mag)	(mag)	
ASASSN-18aay/2018jky							
1456.71	18.139(210)	ASAS-SN
1457.65	17.781(108)	ASAS-SN
1458.75	17.210(073)	ASAS-SN
1459.72	16.912(039)	16.679(027)	16.639(032)	16.881(062)	LCOGT
1459.74	16.718(060)	ASAS-SN
1460.64	16.583(076)	16.449(136)	SMARTS
1461.63	16.264(046)	ASAS-SN
1461.67	16.272(124)	16.131(028)	16.087(043)	16.197(089)	Post O
1462.37	16.023(038)	15.988(030)	15.928(028)	16.122(048)	LCOGT
1462.63	16.030(098)	15.919(136)	SMARTS
1462.74	16.027(041)	ASAS-SN
1463.41	15.892(103)	ASAS-SN
1463.67	15.772(124)	15.760(039)	15.696(049)	15.828(058)	Post O
1464.34	15.676(041)	15.640(027)	15.684(058)	15.828(073)	LCOGT
1464.62	15.694(080)	15.803(198)	SMARTS
1465.63	15.698(042)	ASAS-SN
1466.38	15.533(041)	15.485(037)	15.489(036)	15.733(141)	LCOGT
1466.48	15.700(028)	ASAS-SN
1466.63	15.530(092)	15.514(100)	SMARTS
1467.43	15.658(032)	ASAS-SN
1468.60	15.447(128)	15.360(106)	SMARTS
1468.68	15.425(049)	15.356(041)	15.345(055)	15.761(092)	LCOGT
1469.75	15.524(031)	ASAS-SN
1470.51	...	15.229(134)	15.300(057)	...	LCOGT
1471.80	15.912(117)	ASAS-SN
1472.42	15.552(062)	15.323(033)	15.301(043)	15.822(064)	LCOGT
1472.64	15.582(080)	15.390(099)	SMARTS
1472.75	15.630(054)	ASAS-SN
1473.55	15.539(050)	ASAS-SN
1474.37	15.740(062)	15.438(047)	15.418(045)	16.081(072)	LCOGT
1474.60	15.797(085)	15.467(094)	SMARTS
1475.57	15.884(124)	ASAS-SN
1475.67	15.913(127)	15.486(033)	15.522(053)	16.072(099)	Post O
1476.54	15.954(064)	ASAS-SN
1476.62	16.207(145)	15.707(147)	SMARTS
1476.92	16.072(038)	15.589(063)	15.637(051)	16.224(086)	LCOGT
1477.64	15.840(046)	ASAS-SN
1699.83	...	21.437(108)	22.242(138)	du Pont

Notes. The uncertainties in parentheses are given in thousandths of a magnitude. This table is available in its entirety in machine-readable format in the online journal. A portion is shown here for guidance regarding its form and content.

Table 4. Basic Light-Curve Parameters for SNe Ia in the Sample

SN	$t_{\text{peak}}(B)$ (mag)	B_{peak} (mag)	$\Delta m_{15}(B)$ (mag)	$t_{\text{peak}}(V)$ (mag)	V_{peak} (mag)	$\Delta m_{15}(V)$ (mag)
2015F	108.4±0.7	13.34±0.02	0.73±0.05
2015bp	112.3±0.3	13.87±0.02	1.62±0.08	113.5±0.6	13.88±0.01	0.91±0.05
ASASSN-15jo	168.4±1.2	15.70±0.04	1.76±0.15
ASASSN-15kp	189.0±1.2	15.54±0.03	0.96±0.13	189.4±2.2	15.52±0.05	0.55±0.13
PSN J11492548-0507138	217.1±0.5	13.24±0.03	0.66±0.15
2015aw	227.4±0.6	15.55±0.03	0.93±0.11
ASASSN-15pl	290.5±1.0	15.12±0.03	0.74±0.06
ASASSN-15pz	307.2±0.8	14.23±0.02	0.67±0.08	307.3±0.6	14.23±0.02	0.39±0.04
ASASSN-15qc	299.6±1.0	15.86±0.02	1.05±0.11	303.5±0.4	15.60±0.01	0.72±0.04
2015ao	307.7±0.5	17.48±0.02	1.85±0.12	310.4±0.2	16.81±0.02	1.47±0.05
ASASSN-15rq	324.5±0.4	15.45±0.01	0.84±0.05	325.9±0.4	15.43±0.01	0.55±0.03
ASASSN-15so	350.5±0.8	13.79±0.02	0.94±0.08
2015ar	352.0±0.4	15.35±0.02	1.51±0.08	353.9±0.3	15.25±0.02	0.94±0.04
PSN J21505094-7020289	360.2±0.4	15.49±0.02	1.41±0.07	362.1±0.4	15.09±0.02	0.82±0.04
ASASSN-15ti	364.6±0.5	16.31±0.03	1.37±0.10	366.6±0.8	16.14±0.02	...
2015bd	348.3±0.8	15.19±0.03	0.65±0.06
ASASSN-15uh	388.1±0.8	15.68±0.05	0.92±0.11	390.5±0.8	15.37±0.04	0.59±0.11
ASASSN-15ut	393.1±0.4	16.37±0.02	0.99±0.11
2016F	408.1±0.5	15.15±0.03	0.71±0.07
2016adi	434.0±0.4	15.42±0.03	0.77±0.04
2016bfu	470.7±0.4	16.19±0.03	1.96±0.04	473.2±0.2	15.61±0.01	1.27±0.03
2016blc	490.3±0.7	14.71±0.03	0.99±0.10	490.9±0.9	14.72±0.03	0.64±0.06
2016bln	498.8±0.7	16.00±0.03	0.84±0.09	500.8±1.0	15.92±0.02	0.65±0.07
2016bry	511.8±0.4	15.73±0.02	1.04±0.05
2016ccz	537.1±0.6	15.41±0.03	1.16±0.08	539.4±1.0	15.33±0.03	0.63±0.08
2016coj	547.7±0.2	13.14±0.01	1.34±0.03	548.5±0.3	13.14±0.01	0.70±0.02
2016cqz	555.5±0.6	14.92±0.03	0.78±0.06
2016daj	593.1±0.7	16.61±0.04	1.07±0.10	593.1±1.6	16.63±0.03	0.55±0.11
2016eiy	608.1±0.2	14.42±0.02	1.12±0.03	609.5±0.5	14.19±0.03	0.72±0.06

Notes. This table is available in its entirety in machine-readable format in the online journal. A portion is shown here for guidance regarding its form and content.

APPENDIX

A. OBSERVING PROTOCOL

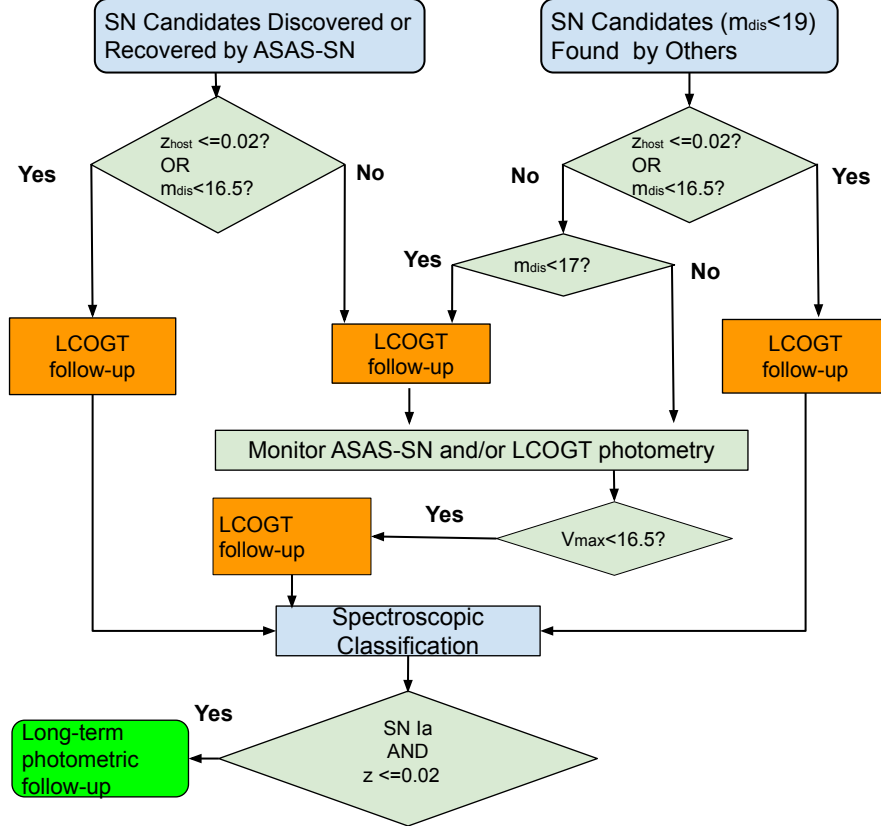


Figure 4. Observing protocol for the CNIa0.02 complete sample.

Fig. 4 illustrates the protocol in our observing procedures when collecting the CNIa0.02 complete sample in the period between 2016 October and 2019 January. We scan the ASAS-SN transient page⁴, the Astronomer’s Telegrams (ATel⁵), the Transient Name Server (TNS⁶), and the Bright Supernova webpage⁷ on a daily basis, and record all bright transients with discovery magnitudes of $m_{\text{dis}} < 19$. To get early follow-up data for SNe Ia in the sample, we start observations before classification for all potential targets according to the strategy in Figure 4. Meanwhile, we coordinate all available spectroscopic resources to classify the potential targets. Note that the primary aim of our complete sample is to include all spectroscopic sub-classes (e.g., 1991bg-like, 1991T-like) that belong to the SNe Ia population. We made follow-up observations of some SNe Ia-like objects (e.g., SNe Iax) that are known to deviate from the WLR of SNe Ia, and they do not belong to the complete sample.

⁴ <http://www.astronomy.ohio-state.edu/~assassin/transients.html>

⁵ <http://www.astronomerstelegam.org/>

⁶ <https://wis-tns.weizmann.ac.il/>

⁷ <http://www.rochesterastronomy.org/snimages/>

Table 5. List of observatories with LCOGT telescopes designed for science operations.

Site Location	Site Code	#2 m	# 1 m	#0.4 m
Siding Spring, Australia	coj	1	2	2
Sutherland, South Africa	cpt		3	1
Teide, Spain	tfn			2
Cerro Tololo, Chile	lsc		3	2
McDonald Observatory, USA	elp		2	1
Haleakala, Hawaii, USA	ogg	1		2

Table 6. Instrument specifications

Imager	Format (pixels)	Binning (pixels)	Pixel scale (arcsec/pixel)	Field of view (arcmin \times arcmin)	Read Noise (e^-)	Gain (e^- /ADU)
SBIG STX-16803	4096 \times 4096	2 \times 2	0.464	15.8 \times 15.8	13.5	1.5
Sinistro	4096 \times 4096	1 \times 1	0.389	26.5 \times 26.5	7–8	1.0
Apogee Alta U230	2048 \times 2048 ^a	1 \times 1	0.77	13.1 \times 13.1	2.9	12.4
Apogee Alta U47	1024 \times 1024	1 \times 1	0.67	11.4 \times 11.4	2.22	11.2
ANDICAM CCD	2048 \times 2048	2 \times 2	0.371	\sim 6 \times 6	6.5	2.3

^aThe central 1024 \times 1024 pixels were used.

B. FOLLOW-UP INSTRUMENTS

B.1. Telescope

The Las Cumbres Observatory Global Telescope network (LCOGT; [Brown et al. 2013](#)) operates a fleet of robotically-controlled telescopes distributed at six sites covering both hemispheres. LCOGT currently has two 2 m, ten 1 m, and ten 0.4 m telescopes, and their locations and site codes are shown in [Table 5](#). Telescopes of a certain aperture class are equipped with the same set of optical imagers⁸. The majority of LCOGT images for our sample were obtained with 1 m-class telescopes. Each 1 m telescope is equipped with either a “Sinistro” or an SBIG STX-16803 camera. Some images were also taken with 2 m or 0.4 m telescopes for which the photometric results will be available in future data releases.

Two 24-inch CDK24 telescopes operated by the Post Observatory were used mainly for northern objects. One is located at the Sierra Remote Observatories (SRO⁹; California, USA) and the other at Post Observatory Mayhill (New Mexico, USA). Two different cameras were used during our follow-up campaign, an Apogee Alta U230 camera and an Apogee Alta U47 camera. Both cameras are back-illuminated, with similar quantum efficiency $> 90\%$ over a broad region. The U230 camera was used by default at both sites. The telescope at SRO utilized the U230 for almost all images, while

⁸ <https://lco.global/observatory/instruments/>

⁹ <https://www.sierra-remote.com/>

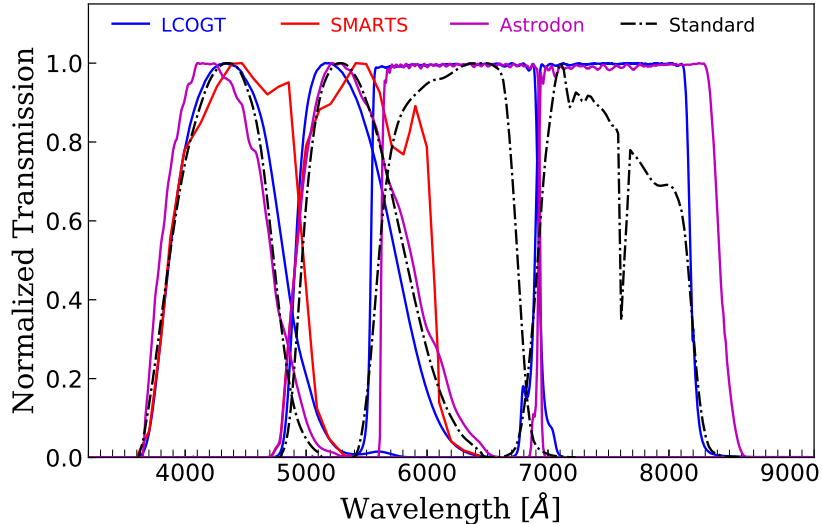


Figure 5. Comparison of filter bandpasses used in this paper (solid lines) with the SDSS r , i and Landolt B , V standard bandpasses (dashed lines).

the Mayhill site had the U47 camera for a long time owing to repair of the damaged shutter of the U230 camera.

The 1.3m telescope of the Small & Moderate Aperture Research Telescope System (SMARTS; Subasavage et al. 2010) equipped with A Novel Dual Imaging CAMera (ANDICAM; DePoy et al. 2003) was used mainly for southern objects. The optical CCD for ANDICAM is a Fairchild 447 2048×2048 pixel CCD. We will publish the near-IR data taken by ANDICAM in a future data release.

B.2. Filters

The LCOGT 1 m telescopes have a standard Johnson-Cousins set ($UBVRI$) and an SDSS/PanSTARRS set ($ugrizy$) of filters. SMARTS/ANDICAM is equipped with standard KPNO-recipe Johnson-Kron-Cousins $BVRI$ filters. Commercial filters are used on the Post Observatory telescopes. Astrodon Photometrics BV^{10} and Sloan ri^{11} filters were used for the images in our sample. The filter set used for observations in this data release are compared to Landolt BV (Landolt 1992) and the SDSS ri (Fukugita et al. 1996) standard bandpasses in Figure 5.

C. PHOTOMETRIC CALIBRATION STANDARDS

For the purpose of homogeneous photometric calibration, photometry from an all-sky reference catalog is preferred to be used for photometric standards. Pan-STARRS1 has carried out multi-band ($grizy_{P1}$) observations of the sky north of declination -30° known as the 3π Steradian Survey (Chambers et al. 2016). Pan-STARRS1 is performed with a well-characterized photometric system, and transformations to other photometric systems are also available (Tonry et al. 2012). The primary calibration standards are selected from the Pan-STARRS1 DR1 MeanObject database table (Flewelling et al. 2016). For the remaining 1/4 of the sky, we use the ATLAS All-Sky Stellar Ref-

¹⁰ <https://astrodon.com/products/astrodon-photometrics-uvbri-filters/>

¹¹ https://astrodon.com/products/astrodon-photometrics-sloan-filters

erence Catalog (Refcat2), which has been assembled from a variety of sources and brought onto the the same photometric system as Pan-STARRS1 (Tonry et al. 2018).

For each image, sources brighter than 19 mag in a given band within the field of the image are extracted. Furthermore, to mitigate contamination from source confusion, radial-exclusion cuts are applied to maximize the number of isolated stars. Lastly, the PS1 or Refcat2 magnitudes are converted to Johnson BV and SDSS ri bands adopting the following transformations (Tonry et al. 2012):

$$\begin{aligned}
 B_{\text{Johnson}} &= g_{\text{PS1}} + 0.212 + 0.556(g_{\text{PS1}} - r_{\text{PS1}}) + 0.034(g_{\text{PS1}} - r_{\text{PS1}})^2, \\
 V_{\text{Johnson}} &= r_{\text{PS1}} + 0.005 + 0.462(g_{\text{PS1}} - r_{\text{PS1}}) + 0.013(g_{\text{PS1}} - r_{\text{PS1}})^2, \\
 r_{\text{SDSS}} &= r_{\text{PS1}} + 0.001 + 0.004(g_{\text{PS1}} - r_{\text{PS1}}) + 0.007(g_{\text{PS1}} - r_{\text{PS1}})^2, \text{ and} \\
 i_{\text{SDSS}} &= i_{\text{PS1}} + 0.005 + 0.011(g_{\text{PS1}} - r_{\text{PS1}}) + 0.010(g_{\text{PS1}} - r_{\text{PS1}})^2.
 \end{aligned}$$